# Physics-based Control-oriented Modeling of the Safety Factor Profile Dynamics in High Performance Tokamak Plasmas

Justin E. Barton, Wenyu Shi, Karim Besseghir, Jo Lister, Arnold Kritz, Eugenio Schuster,
Tim C. Luce, Michael L. Walker, David A. Humphreys and John R. Ferron

***Abstract*— The tokamak is a device that utilizes magnetic fields to confine a reactant gas to generate energy from nuclear fusion reactions. The next step towards the realization of a tokamak power plant is the ITER project, and extensive research has been conducted to find high performance operating scenarios characterized by a high fusion gain and plasma stability. A key property related to both the stability and performance of the plasma is the safety factor profile ($q$-profile). In this work, a general control-oriented physics-based modeling approach is developed, with emphasis on high performance scenarios, to convert the first-principles physics model that describes the $q$-profile evolution in the tokamak into a form suitable for control design, with the goal of developing closed-loop controllers to drive the $q$-profile to a desired target evolution. The DINA-CH&CRONOS and PTRANSP advanced tokamak simulation codes are used to tailor the first-principles-driven (FPD) model to the ITER and DIII-D tokamak geometries, respectively. The model's prediction capabilities are illustrated by comparing the prediction to simulated data from DINA-CH&CRONOS for ITER and to experimental data for DIII-D.**

## I. Introduction

The process of generating energy from nuclear fusion reactions has the potential to have a large impact on the global energy generation landscape. In order for two reactant nuclei to "fuse" together, they must be heated to extremely high temperatures so they possess enough kinetic energy to overcome the Coulombic repulsion force that exists between them. At these temperatures, the reactants (typically deuterium ($D$) and tritium ($T$) in a future reactor-grade device) are in the plasma state, and therefore can conduct electrical current and interact with magnetic fields. The magnetic confinement approach to nuclear fusion energy production is to use externally applied magnetic fields to confine the plasma in a fixed volume and to maintain the conditions necessary for fusion reactions to occur frequently. One of the most promising magnetic confinement devices is the tokamak [1], and the next step towards the realization of a tokamak power plant is the ITER project [2].

Extensive research has been conducted to find high performance operating scenarios that are characterized by a high fusion gain, good plasma confinement, plasma stability, and a noninductively driven plasma current with the goal of developing candidate scenarios for ITER [3]. A key property that is related to both the stability and performance of the plasma is the safety factor profile ($q$-profile) [1]. Recent experiments in the DIII-D tokamak represent the first successful demonstration of first-principles-driven (FPD), model-based, closed-loop control of the entire $q$-profile in a tokamak [4]–[6]. In the DIII-D experiments, the closed-loop control was chosen to be performed in low confinement (L-mode) [1] scenarios due to the reduced complexity of the $q$-profile dynamic model, and hence the model-based control design process, in this regime.

In this work, we convert the first-principles physics model of the poloidal magnetic flux profile evolution [7], which is related to the $q$-profile evolution, in the tokamak into a form *suitable for control design*. This is accomplished by combining the poloidal flux evolution model with simplified control-oriented versions of physics-based models of the electron density and temperature profiles, the plasma resistivity, and the noninductive current-drives, with emphasis on high performance, high confinement (H-mode) [1] scenarios, thereby obtaining a *first-principles-driven* model. This model is developed with the goal of extending the control strategy employed in [4]–[6] to high performance H-mode scenarios.

The objective in developing the simplified physics-based models is to capture the dominant physics that describe how the control actuators affect the respective plasma parameters, and hence the $q$-profile evolution, in H-mode scenarios. High confinement scenarios in tokamaks are characterized by transport barriers [1] just inside the plasma boundary that increase the complexity of the coupling between the magnetic and kinetic plasma states via the increase of the self-generated bootstrap current [8]. Recent progress towards physics-based modeling of the plasma profile evolutions is described in [9]–[11]. The DINA-CH&CRONOS [12] and PTRANSP [13] advanced tokamak simulation codes, which employ complex physics models to predict the plasma dynamics, are employed to obtain simulated data of the plasma evolution to tailor the FPD model to the ITER and DIII-D tokamaks, respectively. The FPD model's prediction capabilities are shown by comparing the prediction to simulated data obtained from DINA-CH&CRONOS for ITER and to experimental data for DIII-D. The tailored models are utilized to design feedback algorithms to control the $q$-profile dynamics in H-mode scenarios in ITER [14] and DIII-D [15] in two companion papers.

This work was supported by the National Science Foundation CAREER Award (ECCS-0645086), the U.S. Department of Energy (DE-FG02-09ER55064) and the Fonds National Suisse de la Recherche Scientifique.
J. Barton (justin.barton@lehigh.edu), W. Shi and E. Schuster are with the Department of Mechanical Engineering and Mechanics, Lehigh University, Bethlehem, PA 18015, USA. K. Besseghir and J. Lister are with the École Polytechnique Fédérale de Lausanne (EPFL), Centre de Recherches en Physique des Plasmas (CRPP), Association EURATOM-Suisse, 1015 Lausanne, Switzerland. A. Krtiz is with the Department of Physics, Lehigh University, Bethlehem, PA 18015, USA. T. Luce, M. Walker, D. Humphreys and J. Ferron are with General Atomics, San Diego, CA 92121, USA.

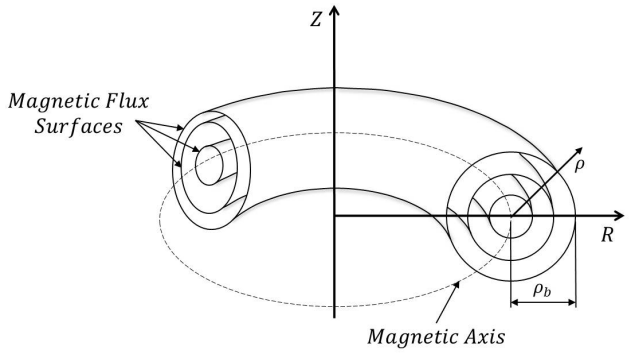


Fig. 1. Magnetic flux surfaces in a tokamak. The limiting flux surface at the center of the plasma is called the magnetic axis. The coordinates $(R,Z)$ define the radial and vertical coordinates in the poloidal plane.

## II. Safety Factor Profile Evolution Model

Any arbitrary quantity that is constant on each magnetic flux surface within the tokamak plasma can be used to index the flux surfaces, which are graphically depicted in Fig. 1. In this work, we choose the mean effective minor radius, $\rho$, of the flux surface, i.e., $\pi B_{\phi,0}\rho^2 = \Phi$, as the indexing variable, where $\Phi$ is the toroidal magnetic flux and $B_{\phi,0}$ is the vacuum toroidal magnetic field at the geometric major radius $R_0$ of the tokamak. The normalized effective minor radius is defined as $\hat{\rho} = \rho/\rho_b$, where $\rho_b$ is the mean effective minor radius of the last closed flux surface. The $q$-profile is related to the poloidal magnetic flux $\Psi$ and is defined as $q(\hat{\rho},t) = -d\Phi/d\Psi = -\left[B_{\phi,0}\rho_b^2\hat{\rho}\right]/\left[\partial\psi/\partial\hat{\rho}\right]$, where $t$ is the time and $\psi$ is the poloidal stream function, which is closely related to the poloidal flux $\Psi$ ($\Psi = 2\pi\psi$). The poloidal magnetic flux evolution is given by the magnetic diffusion equation [7]

$$\frac{\partial\psi}{\partial t} = \frac{\eta(T_e)}{\mu_0\rho_b^2\hat{F}^2}\frac{1}{\hat{\rho}}\frac{\partial}{\partial\hat{\rho}}\left(\hat{\rho}D_\psi\frac{\partial\psi}{\partial\hat{\rho}}\right) + R_0\hat{H}\eta(T_e)\frac{\left\langle\bar{j}_{ni}\cdot\bar{B}\right\rangle}{B_{\phi,0}}, \quad (1)$$

with boundary conditions

$$\left.\frac{\partial\psi}{\partial\hat{\rho}}\right|_{\hat{\rho}=0} = 0 \qquad \left.\frac{\partial\psi}{\partial\hat{\rho}}\right|_{\hat{\rho}=1} = -\frac{\mu_0}{2\pi}\frac{R_0}{\hat{G}\Big|_{\hat{\rho}=1}\hat{H}\Big|_{\hat{\rho}=1}}I_p(t), \quad (2)$$

where $\eta$ is the plasma resistivity, $T_e$ is the electron temperature, $\mu_0$ is the vacuum permeability, $\bar{j}_{ni}$ is any source of noninductive current density, $\bar{B}$ is the magnetic field, $\langle\rangle$ denotes a flux-surface average, $D_\psi(\hat{\rho}) = \hat{F}(\hat{\rho})\hat{G}(\hat{\rho})\hat{H}(\hat{\rho})$, where $\hat{F}$, $\hat{G}$, and $\hat{H}$ are geometric factors pertaining to the magnetic configuration of a particular plasma equilibrium, and $I_p(t)$ is the total plasma current.

## III. Simplified Modeling of Plasma Parameters

The objective in developing the simplified physics-based models of the plasma parameters is to capture the dominant physics that describe how the control actuators (the total plasma current, which is itself controlled by the poloidal field coil system, auxiliary heating/current-drive (H&CD) sources, which are comprised of electron cyclotron (gyrotron), ion cyclotron, and neutral beam launchers, and electron density) affect the parameters, and hence the $q$-profile evolution. The simplified models are developed with particular care being taken to ensure their applicability to H-mode scenarios.

### A. Electron Density Modeling

The electron density profile $n_e(\hat{\rho},t)$ is modeled as

$$n_e(\hat{\rho},t) = n_e^{prof}(\hat{\rho})u_n(t), \quad (3)$$

where $n_e^{prof}(\hat{\rho})$ is a reference profile and $u_n(t)$ regulates the time evolution of the electron density. Note that $n_e^{prof}$ is obtained by evaluating the experimental or simulated $n_e$ at a reference time $t_{r_{n_e}}$, i.e., $n_e^{prof}(\hat{\rho}) = n_e(\hat{\rho},t_{r_{n_e}})$. This model assumes the control action employed to regulate the electron density weakly affects the radial distribution of the electrons.

### B. Electron Temperature Modeling

In the formulation of the electron temperature model, we assume a tight coupling between the plasma electron and ion species, i.e., $T_e(\hat{\rho},t) \approx T_i(\hat{\rho},t)$ and $n_e(\hat{\rho},t) \approx n_i(\hat{\rho},t)$, where $T_i(\hat{\rho},t)$ and $n_i(\hat{\rho},t)$ are the ion temperature and density profiles. The electron temperature profile is modeled as

$$\begin{aligned} T_e(\hat{\rho},t) = {} & k_{T_e}^1(\hat{\rho})\left[T_e^{prof}(\hat{\rho}) - T_e^{prof}(\hat{\rho}_{tb})\right]I_p(t)^\gamma P_{tot}(t)^\varepsilon n_e(\hat{\rho},t)^\zeta \\ & + k_{T_e}^2(\hat{\rho}_{tb})^\omega T_e^{prof}(\hat{\rho}_{tb})I_p(t)^\lambda P_{tot}(t)^\nu n_e(\hat{\rho}_{tb},t)^\xi \end{aligned} \quad (4)$$

in the plasma core ($0 \le \hat{\rho} < \hat{\rho}_{tb}$) and as

$$T_e(\hat{\rho}) = k_{T_e}^2(\hat{\rho})^\omega T_e^{prof}(\hat{\rho})I_p(t)^\lambda P_{tot}(t)^\nu n_e(\hat{\rho},t)^\xi \quad (5)$$

outside of the plasma edge energy transport barrier ($\hat{\rho}_{tb} \le \hat{\rho} \le 1$) [16], where $k_{T_e}^1$ and $k_{T_e}^2$ are constants, $T_e^{prof}(\hat{\rho})$ is a reference profile, $P_{tot}(t)$ is the total power injected into the plasma, and $\hat{\rho}_{tb}$ is the spatial location of the plasma edge energy transport barrier. The constants $\gamma$, $\varepsilon$, and $\zeta$ describe how the temperature in the plasma core scales with the various parameters. The constants $\lambda$, $\nu$, and $\xi$ describe how the temperature outside of the plasma edge transport barrier scales with the various parameters. Note that $T_e^{prof}$ is evaluated at a reference time $t_{r_{T_e}}$, i.e., $T_e^{prof}(\hat{\rho}) = T_e(\hat{\rho},t_{r_{T_e}})$ and the constant $\omega$ is 1 if the temperature outside of the edge transport barrier scales with the various parameters and is 0 otherwise. The constants $k_{T_e}^1$ and $k_{T_e}^2$ are expressed as

$$k_{T_e}^1(\hat{\rho}) = \left[I_p(t_{r_{T_e}})^\gamma P_{tot}(t_{r_{T_e}})^\varepsilon n_e(\hat{\rho},t_{r_{T_e}})^\zeta \mathrm{A}^\gamma\cdot\mathrm{W}^\varepsilon\cdot\mathrm{m}^{(-3)^\zeta}\right]^{-1},$$

$$k_{T_e}^2(\hat{\rho}) = \left[I_p(t_{r_{T_e}})^\lambda P_{tot}(t_{r_{T_e}})^\nu n_e(\hat{\rho},t_{r_{T_e}})^\xi \mathrm{A}^\lambda\cdot\mathrm{W}^\nu\cdot\mathrm{m}^{(-3)^\xi}\right]^{-1},$$

where $k_{T_e}^1$ is defined on the interval $0 \le \hat{\rho} < \hat{\rho}_{tb}$ and $k_{T_e}^2$ is defined on the interval $\hat{\rho}_{tb} \le \hat{\rho} \le 1$.

The total injected power is expressed as $P_{tot}(t) = P_{ohm}(t) + P_{aux}(t) - P_{rad}(t) + \eta_{fus}P_{fus}(t)$, where $P_{ohm}(t)$ is the ohmic power, $P_{aux}(t)$ is the total auxiliary H&CD power, $P_{rad}(t)$ is the radiated power, and $P_{fus}(t)$ is the fusion power. The effectiveness of the fusion power on heating the plasma is captured through the efficiency constant $\eta_{fus}$. The ohmic power is modeled as $P_{ohm}(t) \approx \mathscr{R}_p(t)I_p(t)^2$, where $\mathscr{R}_p(t)$ is the global plasma resistance. The total auxiliary H&CD power is expressed as $P_{aux}(t) = \sum_{i=1}^{n_{ec}}P_{ec_i}(t) + \sum_{i=1}^{n_{ic}}P_{ic_i}(t) + \sum_{i=1}^{n_{nbi}}P_{nbi_i}(t)$, where $P_{ec_i}(t)$ is the individual gyrotron launcher powers, $P_{ic_i}(t)$ is the individual ion cyclotron launcher powers, $P_{nbi_i}(t)$ is the individual neutral beam injector powers, and $n_{ec}$, $n_{ic}$, and $n_{nbi}$ are the total

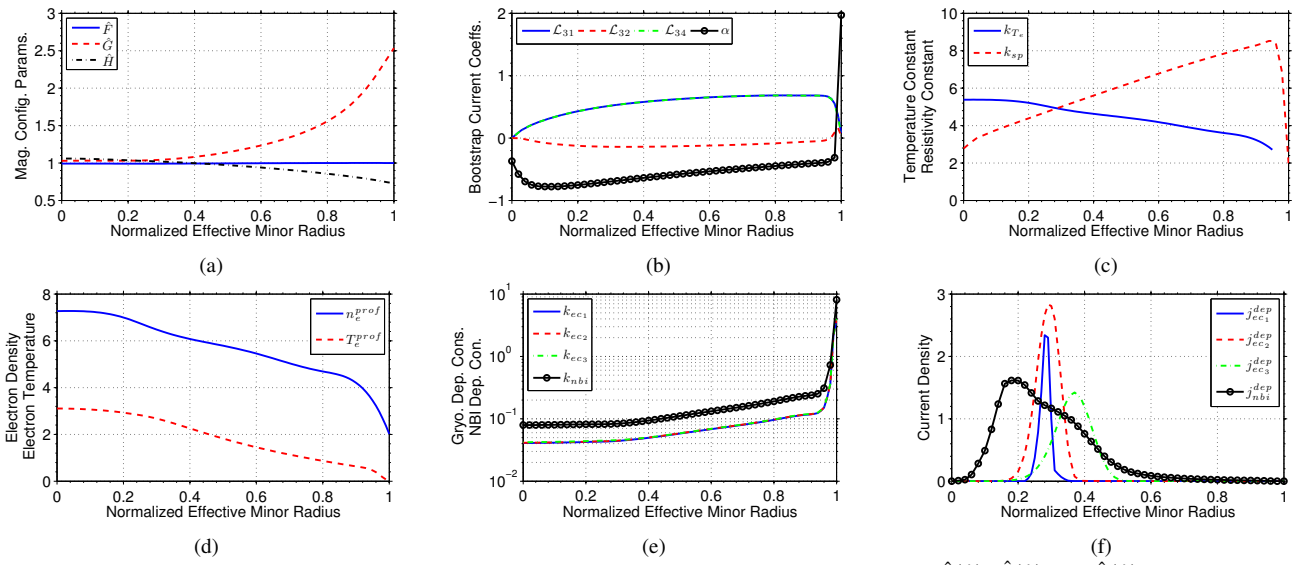


Fig. 2. Model parameters tailored to ITER tokamak: (a) magnetic equilibrium configuration parameters $\hat{F}(\hat{\rho})$, $\hat{G}(\hat{\rho})$ and $\hat{H}(\hat{\rho})$, (b) bootstrap current coefficients $\mathscr{L}_{31}(\hat{\rho})$, $\mathscr{L}_{32}(\hat{\rho})$, $\mathscr{L}_{34}(\hat{\rho})$ and $\alpha(\hat{\rho})$, (c) electron temperature coefficient $k_{T_e} = k_{T_e}^1$ ($10^8$ m$^{-3}$A$^{-1}$W$^{-1/2}$), note $k_{T_e}^2 = 1$, and plasma resistivity coefficient $k_{sp}$ ($10^{-8}$ $\Omega$ m keV$^{3/2}$), (d) reference electron density profile $n_e^{prof}(\hat{\rho})$ ($10^{19}$ m$^{-3}$) and reference electron temperature profile $T_e^{prof}(\hat{\rho})$ ($10^4$ eV), (e) gyrotron model coefficients $k_{ec_1}$, $k_{ec_2}$ and $k_{ec_3}$ ($10^{13}$ m$^{-3}$keV$^{-1}$W$^{-1}$) and neutral beam model coefficient $k_{nbi}$ ($10^{12}$ m$^{-3}$keV$^{-1}$W$^{-1}$), and (f) reference gyrotron current deposition profiles $j_{ec_1}^{dep}(\hat{\rho})$, $j_{ec_2}^{dep}(\hat{\rho})$, and $j_{ec_3}^{dep}(\hat{\rho})$ ($10^5$ A·m$^{-2}$) and reference neutral beam current deposition profile $j_{nbi}^{dep}(\hat{\rho})$ ($10^6$ A·m$^{-2}$).

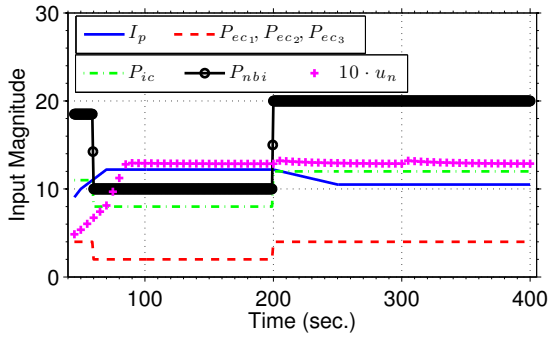


Fig. 3. Control inputs applied during FPD model and DINA-CH&CRONOS simulations (current in MA, power in MW, and $u_n$ is dimensionless).

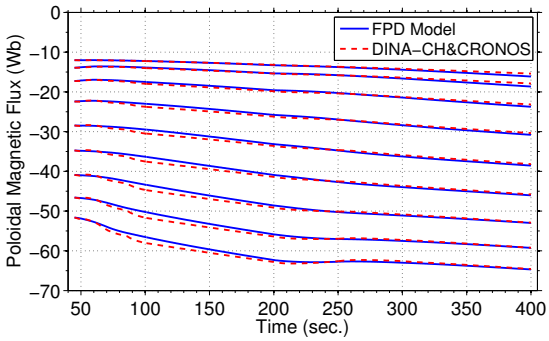


Fig. 4. Time trace of poloidal magnetic flux $\Psi$ at various spatial locations (top to bottom $\hat{\rho} = 0.1, 0.2, \ldots, 0, 8, 0.9$). Note: FPD model (solid) and DINA-CH&CRONOS (dash).

number of gyrotron, ion cyclotron, and neutral beam launchers, respectively. The radiative power density is modeled as $Q_{rad} = k_{brem} Z_{eff} n_e(\hat{\rho},t)^2 \sqrt{T_e(\hat{\rho},t)}$ [1], where $k_{brem} = 5.5 \times 10^{-37}$ Wm$^3/\sqrt{\text{keV}}$ is the Bremsstrahlung radiation coefficient and $Z_{eff}$ is the effective average charge of the ions in the plasma, which we assume to be constant in space and time. The radiated power is then expressed as $P_{rad}(t) = \int_0^1 Q_{rad}(\hat{\rho},t) \frac{dV}{d\hat{\rho}} d\hat{\rho}$, where $V$ denotes the volume enclosed by a magnetic surface within the plasma. The fusion power density is expressed as $Q_{fus}(\hat{\rho},t) = Q_{DT} n_D(\hat{\rho},t) n_T(\hat{\rho},t) \langle \sigma v \rangle_{DT}(\hat{\rho},t) k_{JeV}$ [1], where $Q_{DT} = 17.6$ MeV is the energy released in each $D-T$ reaction, $n_D(\hat{\rho},t)$ and $n_T(\hat{\rho},t)$ are the density of the $D$ and $T$ ions, respectively, and $k_{JeV} = 1.602 \times 10^{-19}$ J/eV. From [17], the $D-T$ reactivity is given by $\langle \sigma v \rangle_{DT} = \exp(\frac{a_1}{T_{DT}^r} + a_2 + a_3 T_{DT} + a_4 T_{DT}^2 + a_5 T_{DT}^3 + a_6 T_{DT}^4)$, where $T_{DT}$ is the $D-T$ temperature in keV and the constants $a_i$ and $r$ are given in [17]. Under our working assumption of an approximately equal electron and ion temperature, we evaluate $\langle \sigma v \rangle_{DT}$ with $T_{DT} = T_e$. The fusion power is then expressed as $P_{fus}(t) = \int_0^1 Q_{fus}(\hat{\rho},t) \frac{dV}{d\hat{\rho}} d\hat{\rho}$.

### C. Plasma Resistivity Modeling

The resistivity $\eta$ scales with the electron temperature as

$$\eta(\hat{\rho},t) = k_{sp}(\hat{\rho}) Z_{eff} / \left[ T_e(\hat{\rho},t)^{3/2} \right], \tag{6}$$

where $k_{sp}(\hat{\rho}) = \left[ \eta(\hat{\rho},t_{r_\eta}) T_e(\hat{\rho},t_{r_\eta})^{3/2} \right] / Z_{eff}$ $\Omega$m(keV)$^{3/2}$ is a constant that is evaluated at a reference time $t_{r_\eta}$.

### D. Noninductive Current-Drive Modeling

The noninductive current-drive is produced by the auxiliary gyrotron and neutral beam launchers and the bootstrap current and is expressed as

$$\frac{\langle \bar{j}_{ni} \cdot \bar{B} \rangle}{B_{\phi,0}} = \sum_{i=1}^{n_{ec}} \frac{\langle \bar{j}_{ec_i} \cdot \bar{B} \rangle}{B_{\phi,0}} + \sum_{i=1}^{n_{nbi}} \frac{\langle \bar{j}_{nbi_i} \cdot \bar{B} \rangle}{B_{\phi,0}} + \frac{\langle \bar{j}_{bs} \cdot \bar{B} \rangle}{B_{\phi,0}}, \tag{7}$$

where $\bar{j}_{ec_i}$ is the noninductive current generated by the individual gyrotron launchers, $\bar{j}_{nbi_i}$ is the noninductive current generated by the individual neutral beam injectors, and $\bar{j}_{bs}$ is the noninductive current generated by the bootstrap effect [8]. In the scenarios considered in this work, the ion cyclotron launchers are configured to only heat the plasma.

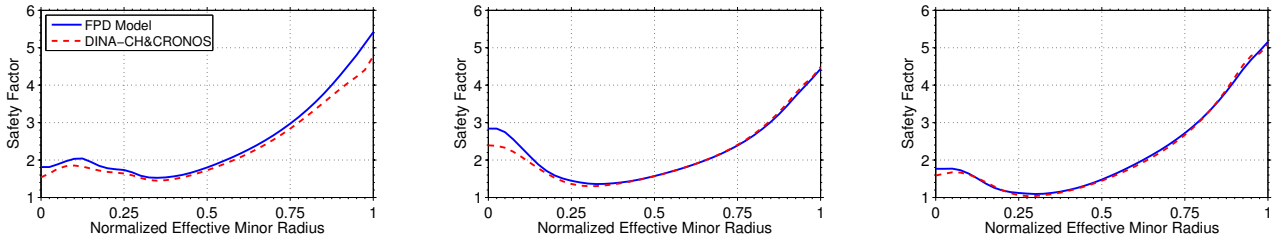


(a) $t = 50$ sec. (b) $t = 150$ sec. (c) $t = 395$ sec.

Fig. 5. Safety factor profile $q(\hat{\rho})$ at various times. Note: FPD model (solid) and DINA-CH&CRONOS (dash).

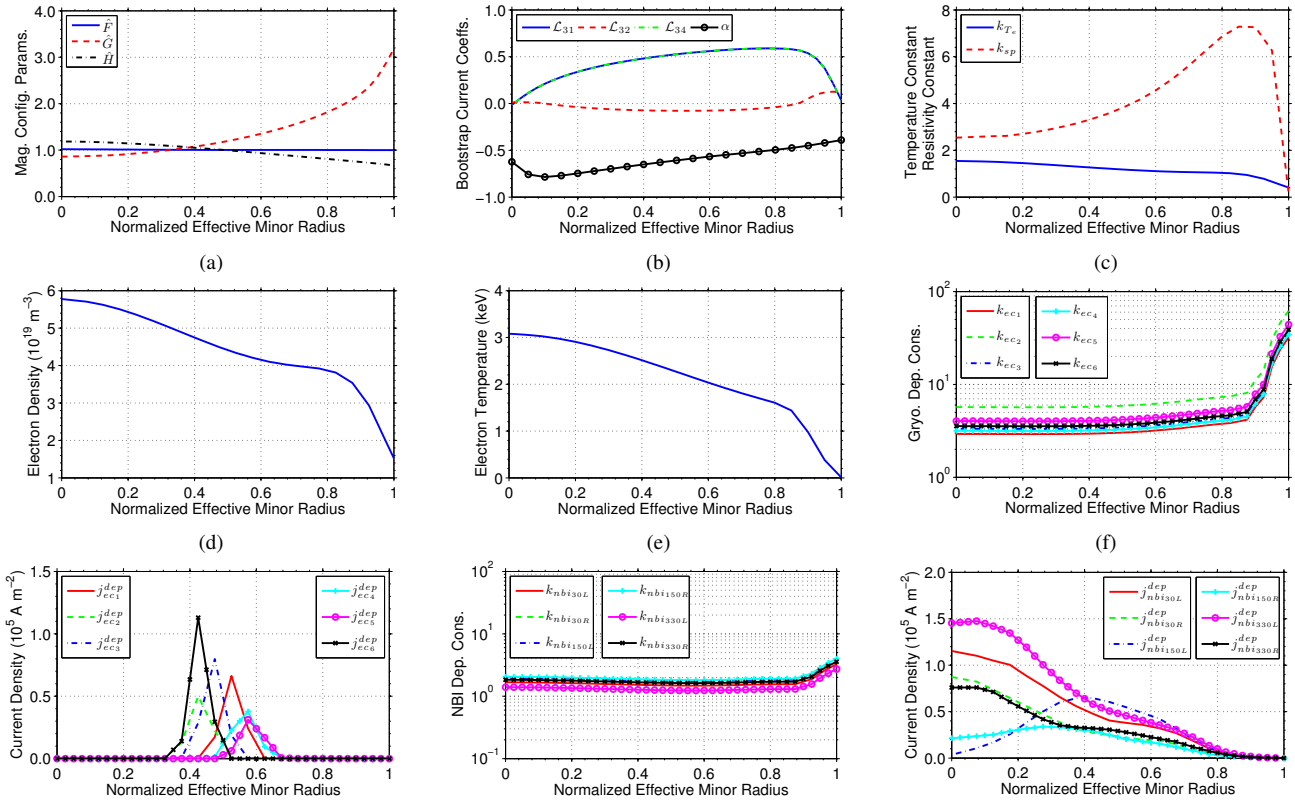


(a) (b) (c) (d) (e) (f) (g) (h) (i)

Fig. 6. Model parameters tailored to DIII-D tokamak: (a) magnetic equilibrium configuration parameters $\hat{F}(\hat{\rho})$, $\hat{G}(\hat{\rho})$, and $\hat{H}(\hat{\rho})$, (b) bootstrap current coefficients $\mathscr{L}_{31}(\hat{\rho})$, $\mathscr{L}_{32}(\hat{\rho})$, $\mathscr{L}_{34}(\hat{\rho})$ and $\alpha(\hat{\rho})$, (c) electron temperature coefficient $k_{T_e} = k^1_{T_e} + k^2_{T_e}$ ($10^{10}$ m$^{-3}$A$^{-1}$W$^{-1/2}$) and plasma resistivity coefficient $k_{sp}$ ($10^{-8}$ $\Omega$ m keV$^{3/2}$), (d) reference electron density profile $n_e^{prof}(\hat{\rho})$, (e) reference electron temperature profile $T_e^{prof}(\hat{\rho})$, (f) gyrotron model coefficients $k_{ec_1},\ldots,k_{ec_6}$ ($10^{13}$ m$^{-3}$keV$^{-1}$W$^{-1}$), (g) reference gyrotron current deposition profiles $j^{dep}_{ec_1}(\hat{\rho}),\ldots,j^{dep}_{ec_6}(\hat{\rho})$, (h) neutral beam model coefficients $k_{nbi_i}$ ($10^{13}$ m$^{-3}$keV$^{-1/2}$W$^{-1}$) for $i \in$ [30L/R,150L/R,330L/R], and (i) reference neutral beam current deposition profiles $j^{dep}_{nbi_i}(\hat{\rho})$ for $i \in$ [30L/R,150L/R,330L/R].

*1) Electron Cyclotron and Neutral Beam Injection Current-Drive:* We model each auxiliary noninductive current-source as the time varying power in each actuator multiplied by a constant deposition profile in space, i.e.,

$$\frac{\langle \bar{j}_i \cdot \bar{B} \rangle}{B_{\phi,0}}(\hat{\rho},t) = k_i(\hat{\rho}) j_i^{dep}(\hat{\rho}) \frac{T_e(\hat{\rho},t)^{\delta}}{n_e(\hat{\rho},t)} P_i(t), \qquad (8)$$

where $i = \left[ec_1,\ldots,ec_{n_{ec}},nbi_1,\ldots,nbi_{n_{nbi}}\right]$, $k_i$ is a normalizing profile, $j_i^{dep}(\hat{\rho})$ is a reference profile for each current-drive source, and the term $T_e^{\delta}/n_e$ represents the current-drive efficiency. For electron cyclotron current-drive, $\delta = 1$ [18] and for neutral beam current-drive, $\delta$ is dependent on the energy of the injected particles [19]. Note that $j_i^{dep}$ is evaluated at a reference time $t_{r_{aux}}$, i.e., $j_i^{dep}(\hat{\rho}) = \left[\langle \bar{j}_i \cdot \bar{B} \rangle / B_{\phi,0}\right](\hat{\rho}, t_{r_{aux}})$. The constants $k_i$ are expressed as $k_i(\hat{\rho}) = n_e(\hat{\rho}, t_{r_{aux}}) / \left[T_e(\hat{\rho}, t_{r_{aux}})^{\delta} P_i(t_{r_{aux}})\right]$ m$^{-3}$/ $\left[\text{keV}^{\delta}\text{W}\right]$ and are also evaluated at a reference time $t_{r_{aux}}$.

*2) Bootstrap Current-Drive:* The bootstrap current arises from the inhomogeneity of the magnetic field strength produced by the external coils in the tokamak, which falls of like $1/R$, and is associated with trapped particles [8]. From [20], we write the bootstrap current as

$$\frac{\langle \bar{j}_{bs} \cdot \bar{B} \rangle}{B_{\phi,0}}(\hat{\rho},t) = \frac{k_{JkeV} R_0}{\hat{F}} \left(\frac{\partial \psi}{\partial \hat{\rho}}\right)^{-1} \left[ 2\mathscr{L}_{31} T_e \frac{\partial n_e}{\partial \hat{\rho}} + \{2\mathscr{L}_{31} + \mathscr{L}_{32} + \alpha \mathscr{L}_{34}\} n_e \frac{\partial T_e}{\partial \hat{\rho}} \right], \qquad (9)$$

where $\mathscr{L}_{31}$, $\mathscr{L}_{32}$, $\mathscr{L}_{34}$, and $\alpha$ depend on the magnetic configuration of a particular plasma equilibrium and $k_{JkeV} = 1.602 \times 10^{-16}$ J/keV.

## IV. Physics-based Control-oriented Model of Poloidal Magnetic Flux Profile Evolution

By combining the simplified physics-based models for the electron density (3) and temperature (4)-(5) profiles, plasma resistivity (6), and noninductive current-drives (7)-(9) with the magnetic diffusion equation (1)-(2), we obtain our desired FPD, physics-based, control-oriented model of the poloidal magnetic flux profile evolution. By defining the control input vector as $u = \left[P_{ec_1},\ldots,P_{ec_{n_{ec}}},P_{ic_1},\ldots,P_{ic_{n_{ic}}},P_{nbi_1},\ldots,P_{nbi_{n_{nbi}}},u_n,I_p\right]$, the FPD model is expressed as

$$\frac{\partial\psi}{\partial t} = f_\eta\left(\hat{\rho},u(t)\right)\frac{1}{\hat{\rho}}\frac{\partial}{\partial\hat{\rho}}\left(\hat{\rho}D_\psi\frac{\partial\psi}{\partial\hat{\rho}}\right)+\sum_{i=1}^{n_{ec}} f_{ec_i}\left(\hat{\rho},u(t)\right)P_{ec_i}(t) + \sum_{i=1}^{n_{nbi}} f_{nbi_i}\left(\hat{\rho},u(t)\right)P_{nbi_i}(t)+f_{bs}\left(\hat{\rho},u(t)\right)\left(\frac{\partial\psi}{\partial\hat{\rho}}\right)^{-1} \quad (10)$$

with boundary conditions

$$\left.\frac{\partial\psi}{\partial\hat{\rho}}\right|_{\hat{\rho}=0} = 0 \qquad \left.\frac{\partial\psi}{\partial\hat{\rho}}\right|_{\hat{\rho}=1} = -k_{I_p}I_p(t), \quad (11)$$

where the parameters $f_\eta$, $f_{ec_i}$, $f_{nbi_i}$, and $f_{bs}$ are functions of the model parameters and $k_{I_p} = \left[\mu_0 R_0\right] / \left[2\pi\hat{G}(1)\hat{H}(1)\right]$.

In the case where the electron temperature in both the plasma core and outside of the edge energy transport barrier scales with the plasma parameters in an identical way, i.e., $\gamma=\lambda$, $\varepsilon=\nu$, $\zeta=\xi$, and $\omega=1$, the spatial and temporal dependence in the model parameters $f_\eta$, $f_{ec_i}$, $f_{nbi_i}$, and $f_{bs}$ can be separated and (10) can be expressed as

$$\frac{\partial\psi}{\partial t} = f_\eta\left(\hat{\rho}\right)u_\eta(t)\frac{1}{\hat{\rho}}\frac{\partial}{\partial\hat{\rho}}\left(\hat{\rho}D_\psi\frac{\partial\psi}{\partial\hat{\rho}}\right)+\sum_{i=1}^{n_{ec}} f_{ec_i}\left(\hat{\rho}\right)u_{ec_i}(t) + \sum_{i=1}^{n_{nbi}} f_{nbi_i}\left(\hat{\rho}\right)u_{nbi_i}(t)+f_{bs}\left(\hat{\rho}\right)u_{bs}(t)\left(\frac{\partial\psi}{\partial\hat{\rho}}\right)^{-1}, \quad (12)$$

where the control inputs are written as

$$\begin{aligned}
u_\eta(t) &= \left[I_p(t)^\gamma P_{tot}(t)^\varepsilon u_n(t)^\zeta\right]^{-3/2}\\
u_{ec_i}(t) &= \left[I_p(t)^\gamma P_{tot}(t)^\varepsilon u_n(t)^\zeta\right]^{-1/2} u_n(t)^{-1}P_{ec_i}(t)\\
u_{nbi_i}(t) &= \left[I_p(t)^\gamma P_{tot}(t)^\varepsilon u_n(t)^\zeta\right]^{(-3/2+\delta)} u_n(t)^{-1}P_{nbi_i}(t)\\
u_{bs}(t) &= \left[I_p(t)^\gamma P_{tot}(t)^\varepsilon u_n(t)^\zeta\right]^{-1/2} u_n(t). \quad (13)
\end{aligned}$$

From (12), we see the magnetic diffusion equation admits actuation not only through interior ($u_{ec_i}, u_{nbi_i}, u_{bs}$) and boundary ($I_p$) control, but also through $u_\eta$, which we name *diffusivity control*. Simulated and/or experimental data can now be used to identify the reference profiles and constants in the simplified physics-based models (3)-(6) and (8)-(9) to tailor the FPD model (10)-(11) to a device and scenario of interest.

## V. Model Tailored to the ITER Tokamak

We employ the DINA-CH&CRONOS free-boundary tokamak simulation code [12] configured to the ITER geometry to obtain simulated data of the plasma evolution to tailor the

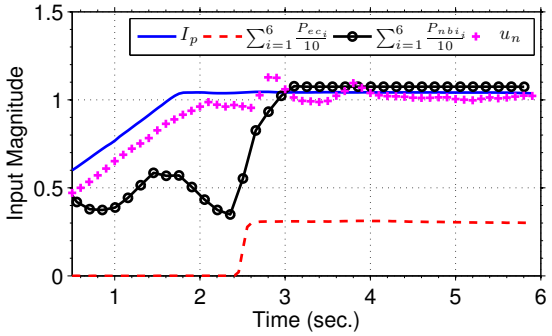


Fig. 7. Control inputs applied during FPD model simulation and DIII-D shot 147634 (current in MA, power in MW, and $u_n$ is dimensionless).

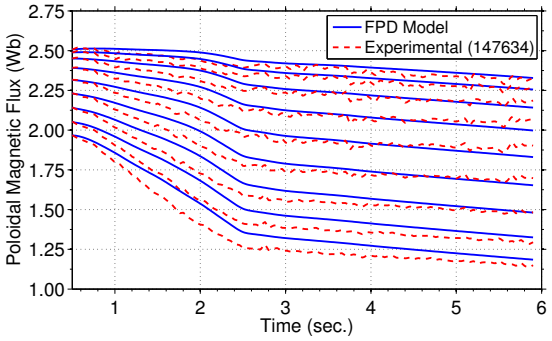


Fig. 8. Time trace of poloidal magnetic flux $\Psi$ at various spatial locations (top to bottom $\hat{\rho} = 0.1, 0.2, \ldots, 0, 8, 0.9$). Note: FPD model (solid) and experimentally achieved in the DIII-D tokamak (dash).

FPD model to H-mode burning plasma scenarios in ITER that have energy and particle transport barriers just inside the plasma boundary. Based on the DINA-CH&CRONOS predicted $T_e$ evolution, the constants in the electron temperature model (4)-(5) are chosen as $\gamma=1$, $\varepsilon=0.5$, $\zeta=-1$ and $\lambda=\nu=\xi=\omega=0$, which models the temperature outside of the edge transport barrier rigidly [16]. The auxiliary H&CD actuators used are 3 independent gyrotron launchers, 1 ion cyclotron launcher, and co-current-injection neutral beam launchers that inject particles at the same radial location. As a result, we group them together to form 1 total neutral beam launcher. The energy of the injected neutral particles on ITER is 1 MeV, therefore, the constant in the neutral beam current-drive model (8) is chosen as $\delta=1$ [19]. The parameters related to the magnetic configuration of the plasma equilibrium and the reference and normalizing profiles for the various models are shown in Fig. 2. The plasma charge neutrality condition is approximated as $n_e(\hat{\rho},t) \approx n_D(\hat{\rho},t)+n_T(\hat{\rho},t) \approx 2n_{DT}(\hat{\rho},t)$, where we have neglected the $D-T$ fusion product and impurity densities and assumed a 50:50 mix of the $D$ and $T$ ions and $n_{DT}$ is the $D-T$ density. Therefore, we choose the fusion heating constant as $\eta_{fus}=0.15$ so the stored energy predicted by the simplified physics-based models matches the stored energy predicted by DINA-CH&CRONOS. The other constants are $B_{\phi,0}=5.3$ T, $R_0=6.2$ m, $\rho_b=2.62$ m, $\hat{\rho}_{tb}=0.95$, and $Z_{eff}=1.7$.

We now describe a simulation study that compares the evolution of the plasma parameters predicted by the FPD model and the DINA-CH&CRONOS free-boundary simulation code [12]. As the FPD model is tailored to the high

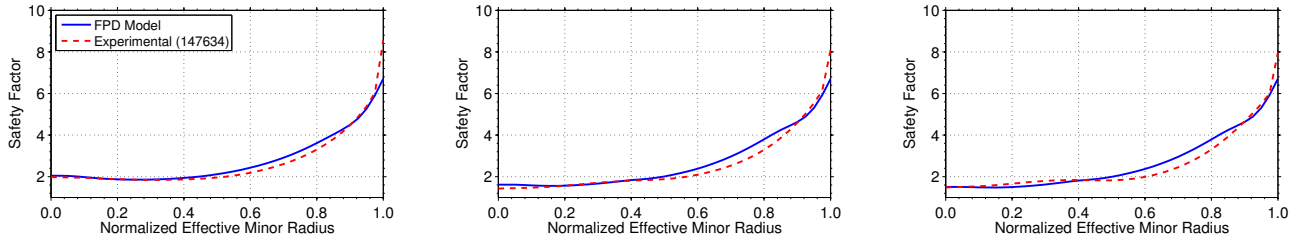


(a) $t = 2.5$ sec. (b) $t = 4.0$ sec. (c) $t = 5.0$ sec.

Fig. 9. Safety factor profile $q(\hat{\rho})$ at various times. Note: FPD model (solid) and experimentally achieved in the DIII-D tokamak (dash).

performance phase of the discharge, we start the simulations just after the plasma transitions from L-mode to H-mode in this particular simulated scenario at the time $t = 45$ sec. The inputs (total plasma current, gyrotron launcher, ion cyclotron launcher, and neutral beam injection powers, and density regulation) applied during both simulations are shown in Fig. 3, time traces of $\Psi$ at various normalized effective minor radii are shown in Fig. 4, and a comparison of the FPD model predicted and DINA-CH&CRONOS predicted $q$-profiles at various times is shown in Fig. 5, respectively. As shown, the trends of the FPD model predicted plasma parameters show good agreement with the DINA-CH&CRONOS results.

## VI. Model Tailored to the DIII-D Tokamak

We employ experimental data and simulated data from the PTRANSP advanced tokamak simulation code [13] configured to the DIII-D geometry to tailor the FPD model to H-mode plasma scenarios in DIII-D that have energy and particle transport barriers just inside the plasma boundary. Based on the experimental $T_e$ evolution, we choose the constants in the electron temperature model (4)-(5) as $\gamma = \lambda = 1$, $\varepsilon = \nu = 0.5$, $\zeta = \xi = -1$, and $\omega = 1$, which scales the temperature profile in the plasma core and outside of the edge transport barrier in the same way with the plasma parameters, and the FPD model takes the form of (12). The auxiliary H&CD actuators on DIII-D considered in this work are 6 independent gyrotron launchers and 6 co-current-injection neutral beam launchers, which inject particles with an energy of 80 keV. Therefore, the constant in the neutral beam current-drive model (8) is chosen as $\delta = 1/2$ [19]. The parameters related to the magnetic configuration of the plasma equilibrium and the reference and normalizing profiles for the various models are shown in Fig. 6. As the plasma in DIII-D is not hot enough to produce a significant probability of fusion reactions occurring, we choose the fusion heating constant as $\eta_{fus} = 0$. The other constants are $B_{\phi,0} = 1.65$ T, $R_0 = 1.6955$ m, $\rho_b = 0.82$ m, and $Z_{eff} = 1.75$.

We now describe a study that compares the evolution of the plasma parameters predicted by the FPD model to the experimentally achieved plasma parameters in DIII-D shot 147634. The inputs (total plasma current, total gyrotron launcher and total neutral beam injection powers, and density regulation) applied during both the simulation and the experiment are shown in Fig. 7, time traces of $\Psi$ at various normalized effective minor radii are shown in Fig. 8, and a comparison of the FPD model predicted and the experimentally achieved $q$-profiles at various times is shown in Fig. 9, respectively. As shown, the trends of the FPD model predicted plasma parameters show good agreement with the experimental results achieved in DIII-D.

## VII. Conclusion and Discussion

We developed a general simplified physics-based modeling approach to convert the first-principles physics model that describes the poloidal magnetic flux profile, and hence the $q$-profile, evolution in the tokamak into a form suitable for control design, with emphasis on high performance operating scenarios. The FPD model's prediction capabilities were demonstrated by comparing the prediction to both simulated data obtained from DINA-CH&CRONOS for ITER and experimental data for DIII-D. Advanced tokamak simulation and experimental testing of controllers [14], [15] designed to control the $q$-profile evolution in H-mode scenarios by employing the FPD model is part of our future work and will help assess the true requirements for model accuracy.

## References


[1] WESSON, J., *Tokamaks*, Oxford, U.K.: Clarendon Press, 1997.
[2] ITER Organization, [Online]. Available: http://www.iter.org.
[3] TAYLOR, T. et al., Plasma Phys. and Control. Fusion **39** (1997) B47.
[4] BARTON, J. E., BOYER, M. D., SHI, W., SCHUSTER, E., et al., Nucl. Fusion **52** (2012) 123018.
[5] BOYER, M. D., BARTON, J. E., SCHUSTER, E., et al., Plasma Phys. Control. Fusion **55** (2013) 105007.
[6] BOYER, M. D., BARTON, J., SCHUSTER, E., et al., Backstepping Control of the Plasma Current Profile in the DIII-D Tokamak, in *American Control Conference Proceedings*, pp. 2996–3001, 2012.
[7] HINTON, F. and HAZELTINE, R., Rev. Mod. Phys. **48** (1976) 239.
[8] PEETERS, A. G., Plasma Phys. and Control. Fusion **42** (2000) B231.
[9] OU, Y., LUCE, T. C., SCHUSTER, E., et al., Fusion Engineering and Design **82** (2007) 1153.
[10] WITRANT, E. et al., Plasma Phys and Control Fusion **49** (2007) 1075.
[11] FELICI, F. et al., Nuclear Fusion **51** (2011) 083052.
[12] KIM, S. H. et al., Plasma Phys. and Control. Fusion **51** (2009) 105007.
[13] HAWRYLUK, R., An Empirical Approach to Tokamak Transport, in *Course on Physics of Plasma Close to Thermonuclear Conditions, Varenna, Italy*, 1979.
[14] BARTON, J. E., BESSEGHIR, K., LISTER, J., and SCHUSTER, E., Robust Control of the Safety Factor Profile and Stored Energy Evolutions in High Performance Burning Plasma Scenarios in the ITER Tokamak, in *52nd IEEE Conference on Decision and Control*, (this conference), 2013.
[15] SHI, W., BARTON, J., WEHNER, W., BOYER, M, SCHUSTER, E, et al., First-principles-driven Control of the Rotational Transform Profile in High Performance Discharges in the DIII-D Tokamak, in *52nd IEEE Conference on Decision and Control*, (this conference), 2013.
[16] ITER Physics Basis, Nuclear Fusion **39** (1999) 2137.
[17] HIVELY, L. M., Nuclear Fusion **17** (1977) 873.
[18] LUCE, T. C. et al., Physical Review Letters **83** (1999) 4550.
[19] POLITZER, P. A. and PORTER, G. D., Nucl. Fusion **30** (1990) 1605.
[20] SAUTER, O. et al., Physics of Plasmas **6** (1999) 2834.